Predicting the physics of ion cyclotron emission from neutral beam-heated plasmas in the Wendelstein 7-X stellarator

O Samant[1], R O Dendy[2,1], S C Chapman[1,3], D Moseev[4] and R Ochoukov[5]

[1]*Centre for Fusion, Space and Astrophysics, Department of Physics, Warwick University, Coventry CV4 7AL, UK*
[2]*CCFE, Culham Science Centre, Abingdon, Oxfordshire OX14 3DB, UK*
[3]*Department of Mathematics and Statistics, University of Tromsø, Norway*
[4]*Max-Planck-Institut für Plasmaphysik, Wendelsteinstr. 1, 17491 Greifswald, Germany*
[5]*Max-Planck-Institut für Plasmaphysik, Boltzmannstr. 2, 85748 Garching, Germany*

1.Introduction

Spontaneously generated radiation in the ion cyclotron range of frequencies (ion cyclotron emission (ICE), associated with neutral beam injection (NBI) of energetic ions into the KSTAR[1] and DIII-D[2] tokamaks and the LHD heliotron-stellarator[3], is caused by collective relaxation of the NBI ions undergoing the magnetoacoustic cyclotron instability (MCI). The ICE spectrum typically has strongly suprathermal peaks at harmonics of the local ion cyclotron frequency in the edge plasma. Edge NBI ICE has been simulated in Refs.[1-3] from first principles, using particle-in-cell (PIC) kinetic codes which solve the Maxwell-Lorentz system of equations self-consistently for tens of millions of gyro-orbit-resolved particles. Comparison between ICE spectra from tokamaks and stellarators sheds light on the relative importance of overall magnetic field structure compared to spatially localised physics. Here we report PIC simulations that predict ICE spectra from imminent observations from NBI-heated plasmas in the Wendelstein 7-X stellarator. These simulations are computationally resource-intensive, partly due to the low ratio of the perpendicular velocity of the NBI ions to the local Alfvén velocity, V_{NBI}/V_A=0.14, requiring typically 200,000 CPU-hours apiece. Our simulations capture the full frequency range from ion cyclotron through lower hybrid and beyond, with high resolution. It appears that both the MCI and the lower hybrid drift instability, found in related simulations[4,5], may operate simultaneously in the Wendelstein 7-X scenario. They may be manifestations of a single underlying plasma phenomenon at the level of first principles kinetics. The development of a predictive capability, in addition to interpretive, for linking the spectral structure of ICE to the velocity-space structure of the emitting ion population is important for the diagnostic exploitation of ICE in present and future fusion experiments.

2.Simulation Results

We use the 1D3V EPOCH[6] PIC code to simulate the system. The electrons and majority protons form the thermal background. The minority fast ions representing the NBI protons are initialised as a drifting ring-beam distribution given by $f(v_\parallel, v_\perp) \propto \exp\left(-\frac{(v_\parallel - v_d)^2}{v_r^2}\right) \exp\left(-\frac{(v_\perp - u_0)^2}{u_r^2}\right)$. The system is then allowed to relax. Magnetic field data from the simulation is used to calculate the spatiotemporal Fourier transform, as shown in Fig.1(left) for the case with wave propagation at 89.5° with respect to the magnetic field **B**. Here the component B_z is chosen, because it is perpendicular to the simulation direction and hence the **k**-vector, thus capturing the electromagnetic physics of the system. Figure

1(left) shows that the spontaneously excited fields are concentrated in distinct regions of (ω,k) space: spectrally peaked at the 2nd ion cyclotron harmonic; and broadband between dimensionless wavenumbers $k = 10$ to 30, and $k = 50$ to 60 (hereafter the "blob") close to the lower hybrid frequency ω_{LH}. Integrating over k-space yields the frequency power spectrum, Fig.1(right). Multiple simulations (Fig.2) for quasi-perpendicular propagation at angles between $85°$ and $89.5°$ to $\boldsymbol{B}$ show that the excitation of spectral peaks at the 2nd and 3rd harmonics is a robust feature. This is a key prediction of the present work.
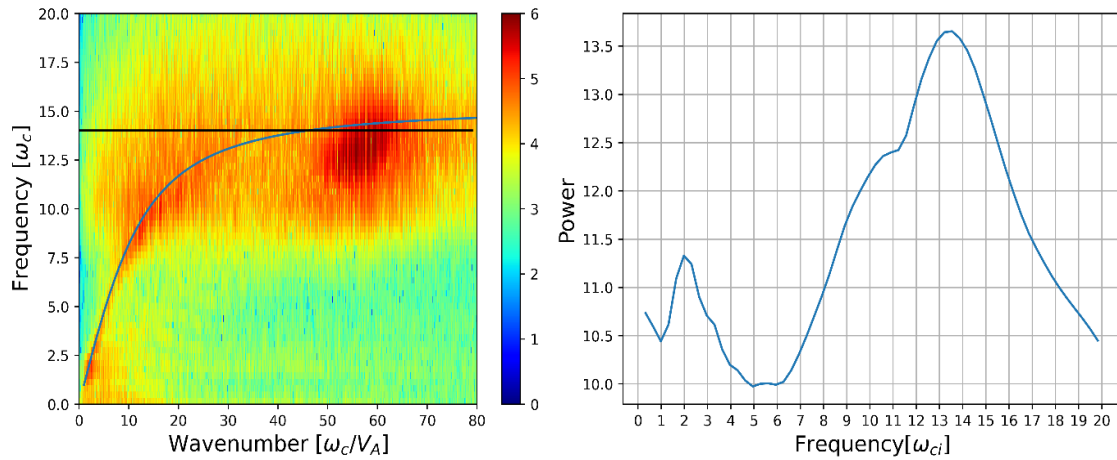

Fig.1 Left: Spatiotemporal FFT of Z component of magnetic field(B_z) showing the distribution of energy across frequency-wavenumber space, with frequencies normalised to the ion cyclotron frequency and the wavenumbers normalised to the ratio of ion cyclotron frequency to Alfven velocity. Shading indicates the $\log_{10}$ of the spectral density. The blue line shows the cold plasma dispersion relation, and the black line is the lower hybrid frequency. **Right:** Corresponding power spectra obtained by summing, over all k, the power at each frequency in the 2D FFT.
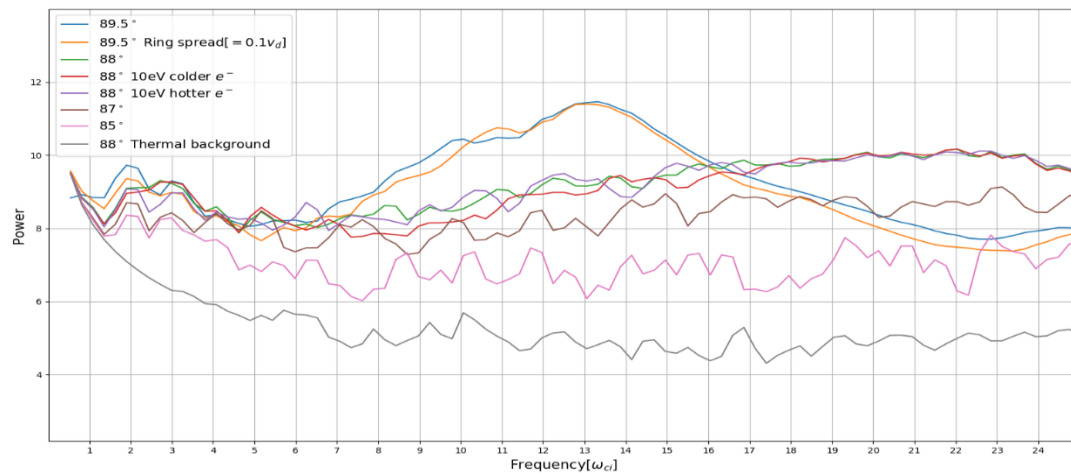

Fig.2 Log_{10} plot of spectral intensity of predicted ICE. Coloured lines are for different angles of wave propagation with respect to $\boldsymbol{B}$, together with dependence on spread in the ring beam of fast ions (orange), and on electron temperature (red and purple). The grey line shows the baseline spectrum from a simulation containing no suprathermal ions, determined by the thermal background. The 2nd and 3rd harmonic peaks arise in all cases with a ring-beam, together with harmonics 4, 5 and 6 in some of them. The "blob" spans harmonics 8 to 18 in the $89.5°$ cases; 20 to 23 for $88°$; and is off scale to the right in the $87°$ and $85°$ cases.

Figure 3 was obtained by stacking the 1D FFTs of magnetic field component B_z in each cell at different times. The blob grows first, before the ICE at lower harmonics, and dies out around the time when the lower harmonics gain energy. This suggests the "blob" may drive the ICE the lower harmonics, energy being transferred by conjectured nonlinear coupling which we will test, using bispectral methods, in future work.

Figure 4 shows the change in energy densities in the field components E_x and B_z and in the different particle populations. In this sub-Alfvénic regime for the NBI ions, it is expected from previous analyses of observations of NBI-driven ICE [1,7,8] that the MCI will include a significant electrostatic component. This is seen here in Fig.4, where the initial rise is at times corresponding to the growth of field energy at $\omega \approx \omega_{LH}$ in Fig.3. This transitions at $t = 1.25\ \tau_{gp}$ in Figs.3 and 4 to the growth of spectral peaks at lower ion cyclotron harmonics. The extent to which the high-frequency electrostatic regime of the MCI is distinguishable from the LHDI (cf. the PIC studies in Refs.[4,9]) is under investigation.
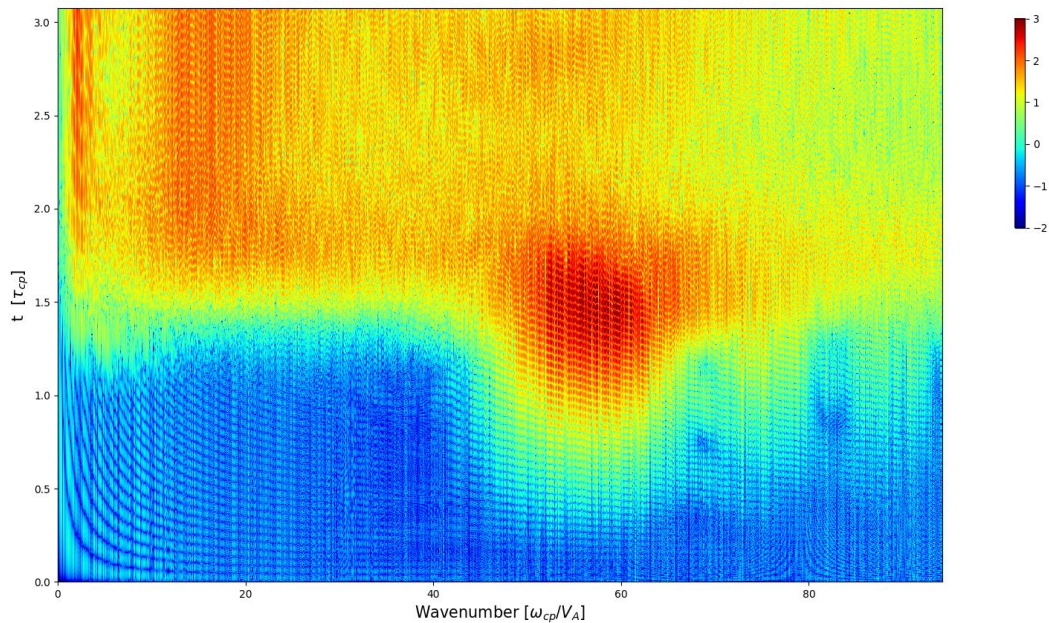

Fig.3 Time evolution of 1D spatial FFT of magnetic field component B_z. This shows the variation of the energy distribution across different wavenumbers (normalised to the ratio of ion cyclotron frequency to the Alfven velocity) at different points in time (normalised to the ion gyroperiod). The "blob", located approximately between wavenumbers 45 and 65, starts around $0.5\tau_{gp}$. This is well before the spectral peaks at the 2nd and 3rd harmonics, which rise around $1.25\tau_{gp}$, while the "blob" declines.

3.Conclusions and future work
We predict the excitation of ICE spectral peaks at the 2nd and 3rd proton cyclotron harmonics in the edge region of H plasmas heated by H NBI in the W7-X stellarator. The predominantly electrostatic character that we predict for these ICE peaks suggests that they
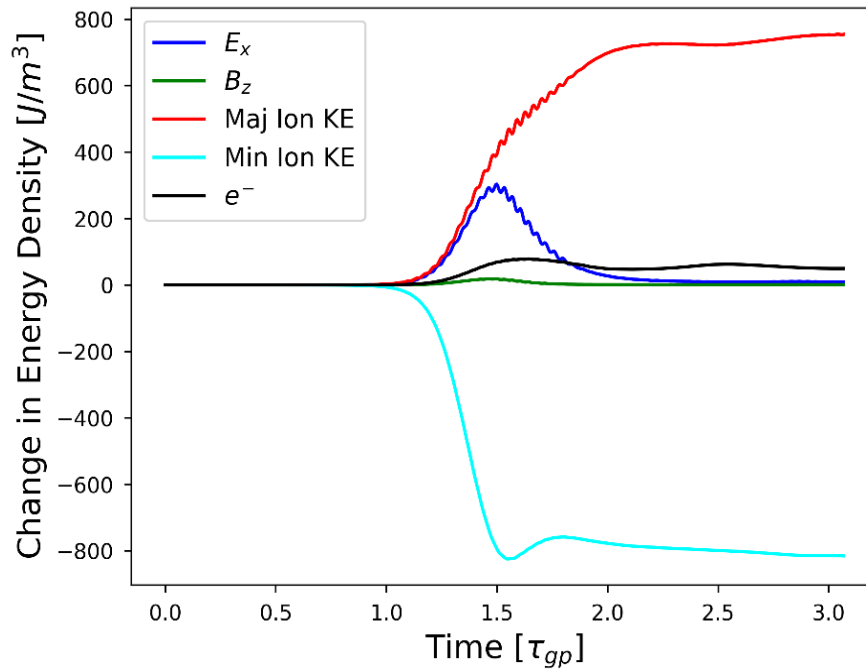
Fig.4 Time evolution of change in energy densities of particles, electric field E_x and magnetic field B_z in the 89.5° case. The MCI starts around $t = \tau_{gp}$, which matches Fig.3, and is predominantly electrostatic, with the energy excited in E_x significantly greater than in B_z.

could be detectable with probes, as previously in TFTR [7,10], as well as antennas. The lower cyclotron harmonics in our simulation may be driven by nonlinear interactions within the "blob" structure, which is excited at frequencies closer to the lower hybrid frequency. The excitation of the "blob", involving radiation at frequencies comparable to the lower hybrid frequency, is our second main prediction. Planned calculation of the bicoherence and bispectrum of the fields excited in our simulations will quantify three-wave nonlinear energy transfer during the phases where linear-type modes exist.

References

[1] Chapman, B., et al. *Nuclear Fusion* **59**.10 (2019): 106021.
[2] Zalzali, A., Thome, K.E., et al, 47th EPS Conference on Plasma Physics P4.1002
[3] Reman, B. C. G., et al. *Nuclear Fusion* **59**.9 (2019): 096013.
[4] Cook, J. W. S., S. C. Chapman, and R. O. Dendy. *Physical Review Letters* **105**.25 (2010): 255003.
[5] Cook, J. W. S., et al. *Plasma Physics and Controlled Fusion* **53**.6 (2011): 065006.
[6] Arber, T. D., et al. *Plasma Physics and Controlled Fusion* **57**.11 (2015): 113001.
[7] Dendy, R. O., et al. *Physics of Plasmas* **1**.10 (1994): 3407.
[8] Reman, B. C. G., et al. *Nuclear Fusion* **61**.6 (2021): 066023.
[9] Cook, J. W. S., Dendy, R.O. et al. *Plasma Physics and Controlled Fusion* **53**.7 (2011): 074019.
[10] Cauffman, S., et al. *Nuclear Fusion* **35**.12 (1995): 1597.

Acknowledgements